A Homeostasis Criterion for Limit Cycle Systems Based on Infinitesimal Shape Response Curves

Zhuojun Yu[1] & Peter J. Thomas[1−5]
[1]Department of Mathematics, Applied Mathematics and Statistics
[2]Department of Biology, [3]Department of Cognitive Science,
[4] Department of Computer and Data Science
[5]Department of Electrical, Control and Systems Engineering
Case Western Reserve University, Cleveland, Ohio 44106 (USA)

August 28, 2022

We mark new text in red font.

Abstract

Homeostasis occurs in a control system when a quantity remains approximately constant as a parameter, representing an external perturbation, varies over some range. Golubitsky and Stewart (J. Math. Biol., 2017) developed a notion of infinitesimal homeostasis for equilibrium systems using singularity theory. Rhythmic physiological systems (breathing, locomotion, feeding) maintain homeostasis through control of large-amplitude limit cycles rather than equilibrium points. Here we take an initial step to study (infinitesimal) homeostasis for limit-cycle systems in terms of the *average* of a quantity taken around the limit cycle. We apply the "infinitesimal shape response curve" (iSRC) introduced by Wang et al. (SIAM J. Appl. Dyn. Sys, 2021) to study infinitesimal homeostasis for limit-cycle systems in terms of the *mean* value of a quantity of interest, averaged around the limit cycle. Using the iSRC, which captures the linearized *shape* displacement of an oscillator upon a static perturbation, we provide a formula for the derivative of the averaged quantity with respect to the control parameter. Our expression allows one to identify homeostasis points for limit cycle systems in the averaging sense. We demonstrate in the Hodgkin-Huxley model and in a metabolic regulatory network model that the iSRC-based method provides an accurate representation of the sensitivity of averaged quantities.

Keywords: limit cycle, motor control, homeostasis, variational method, ordinary differential equations, sensitivity analysis

ORCID ID:
Zhuojun Yu: https://orcid.org/0000-0002-4243-2405
Peter J. Thomas: https://orcid.org/0000-0001-7533-6770
Contact e-mail: ZY: zhuojun.yu@case.edu†, PJT: pjthomas@case.edu.
†: Corresponding author.

1 Introduction

> "tous les mécanismes vitaux, quelque variés qu'ils soient, n'ont toujours qu'un but, celui de maintenir l'unité des conditions de la vie dans le milieu intérieur."[1]

[1] "all the vital mechanisms, however varied they may be, have only one object, that of preserving constant the conditions of life in the internal environment" – quoted in translation by [8].

— Claude Bernard [4], p. 121

Many problems in control, particularly in physiological systems, involve holding a quantity steady despite variation of external conditions. Examples include stabilization of body temperature against changes in external temperature [29, 30], maintenance of metabolite concentrations in the face of fluctuating metabolic demands [31, 34], and stabilization of blood pressure under changes of body posture [23, 32]. This form of robustness against sustained external perturbations is called *homeostasis* [8]. Understanding mechanisms of homeostasis is an important aspect of biological systems analysis.

In many instances, homeostasis involves a dynamical system with trajectories that converge to a stable equilibrium point. As a parameter is varied, representing the external perturbation, the location of the fixed point in an n-dimensional state space may shift, while the value of one component of interest – representing the controlled quantity – remains approximately constant. In this setting, there is a well developed theory for homeostasis based on singularity theory, developed by Golubitsky and Stewart [15, 16, 22]. These authors formulate "infinitesimal homeostasis" as the condition that the derivative of a particular component of the steady-state solution with respect to the input parameter should vanish. This theory has been successfully applied to a variety of biochemical and metabolic systems, each having a unique stable equilibrium for each value of the input [2, 34].

In contrast, in many physiological systems, the "locus of control" is not a dynamical fixed point but rather a stable limit cycle. For example, in order to maintain approximately constant concentrations of oxygen and carbon dioxide in the blood, the mammalian respiratory central pattern generator produces ongoing large amplitude rhythmic activity that drives the biomechanics of the airways and lungs [7, 9, 12, 14, 18, 35, 36, 37]. Other examples include locomotion [1, 3, 19, 41], in which the "objective" may be thought of as moving the center of mass forward at a steady rate, despite variations in viscosity or steepness of terrain; and swallowing [26, 38, 42], with the quantity to be held constant representing the rate of intake of food, and the perturbation coming from variable resistance of the food to being consumed. In general, the quantity of interest may vary during each period of the limit cycle; in this paper we will assume the *mean value* of some specified state space variable, averaged around the limit cycle, is the quantity that is subject to control.

The singularity theoretic methods developed by Golubitsky and Stewart for studying infinitesimal homeostasis do not directly apply to systems in which the underlying dynamics is oscillatory, except in special cases. The authors of [10, 11], for example, investigated a system undergoing a supercritical Hopf bifurcation, creating a small-amplitude limit cycle upon loss of stability of an equilibrium point, as the input parameter varied. For certain examples of both feedback- and feedforward-regulatory systems, the oscillatory output variable still remained near a homeostatic plateau.

It would be desirable to develop a theory parallel to that established by Golubitsky and Stewart for systems in which the locus of control involves a limit cycle of unrestricted amplitude. To emphasize the difference between fixed-point homeostasis and general limit-cycle homeostasis, Fig. 1 shows a one-parameter family of limit cycles generated by the Hodgkin-Huxley equations subject to a range of different driving currents. (See §3.2 for the HH equations.) As the injected current I increases from 10 picoAmperes up to 150 pA, the period of the limit cycle decreases and its shape – meaning the geometry of the point set corresponding to the closed loop of the trajectory – changes as well. Thus, whereas identifying fixed-point homeostasis only requires tracking the change in a scalar component of a static equilibrium under parameter changes, investigating homeostasis in a limit-cycle system potentially requires tracking changes in both

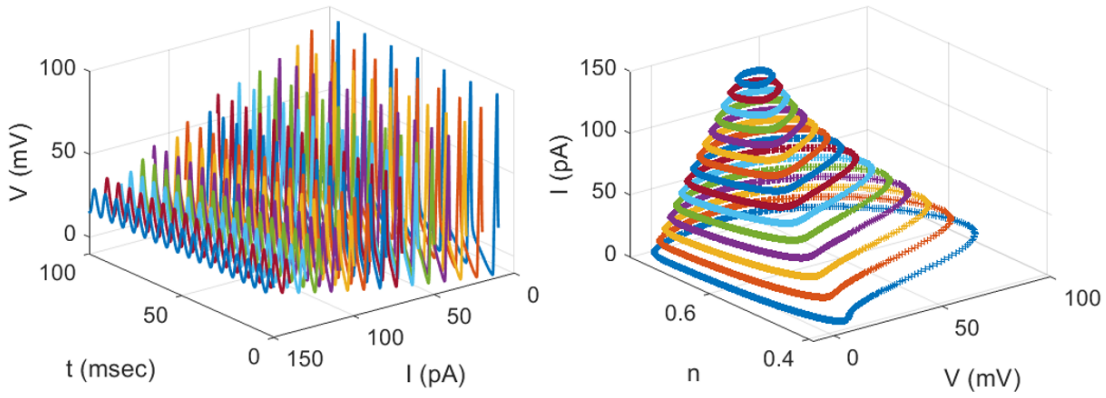

Figure 1: One-parameter family of limit cycles generated by the Hodgkin-Huxley equations for different values of the driving current I. Cf. (20) in §3.1. **Left:** Voltage (V) as a function of time for $10 \leq I \leq 150$ pA. **Right:** Closed orbits in the (V, n) plane for different values of applied current I. Note that as the current increases, both the timing (period) and the shape of the orbits changes.

shape and timing of the orbit.

In this paper we take a first step towards a theory of homeostasis for limit cycle systems, by analyzing how the average of an arbitrary quantity responds to a sustained change in a parameter influencing the limit cycle dynamics. We find that the key quantity in the analysis is the *infinitesimal shape response curve* (iSRC) recently introduced in [42]. The iSRC complements the well-known infinitesimal phase response curve (iPRC). The latter quantifies, to linear order, the effect of an instantaneous perturbation on the timing of the limit cycle, and also captures the cumulative effect of a sustained perturbation on the limit cycle period. In contrast, the iSRC captures the effect of a sustained or parametric perturbation on the *shape* of a limit cycle trajectory, to linear order.

As the main contribution of the paper, we give a formula for calculating the derivative of the average of any physical quantity of interest with respect to a sustained perturbation, provided the quantity and the underlying dynamical system are sufficiently smooth. The iSRC as introduced by [42] is actually a family of curves related by an arbitrary phase shift (much as the asymptotic phase function of a limit cycle oscillator is defined only up to an arbitrary phase shift). As a second contribution, we show here that the arbitrary phase shift associated with the iSRC drops out when calculating the sensitivity of a quantity of interest averaged around the limit cycle. This result clarifies the (in)significance of the ambiguity arising naturally in the definition of the iSRC, and comports with physical intuition: the sensitivity of a well defined average should not depend on the coordinate system in which the sensitivity is measured.

After specifying the mathematical framework of the problem, and establishing our technical results, we apply the iSRC analysis to two smooth example systems. First, we calculate the iSRC for the well-known Hodgkin-Huxley model for action potential generation in the squid giant axon, and show that we can accurately find the sensitivities of quantities such as the mean voltage, the mean sodium current and the mean potassium current. Then, we calculate the iSRC for two metabolic regulatory networks undergoing Hopf bifurcation, and compare our results with those of [10]. In both cases we find excellent agreement between the sensitivities calculated by the iSRC-based method and direct numerical finite difference calculations.

2 Mathematical formulation

Consider a one-parameter family of smooth dynamical systems on a domain $\mathcal{D}$ in $\mathbb{R}^n$,

$$\frac{d\mathbf{x}}{dt} = \mathbf{F}(\mathbf{x}, \epsilon) \tag{1}$$

with state vector $\mathbf{x} \in \mathcal{D} \subset \mathbb{R}^n$, parametrized by $\epsilon \in \mathcal{I} \subset \mathbb{R}$ representing a (static) perturbation. We make the following assumptions:

A1 The vector field $\mathbf{F}$ is continuously differentiable in both $\mathbf{x}$ and ϵ, i.e. the derivatives $\nabla_{\mathbf{x}}\mathbf{F}$, $\partial\mathbf{F}/\partial\epsilon$, $\partial\nabla_{\mathbf{x}}\mathbf{F}/\partial\epsilon$ and $\nabla_{\mathbf{x}}\left(\partial\mathbf{F}/\partial\epsilon\right)$ are well defined continuous functions for $\mathbf{x} \in \mathcal{D}$ and $\epsilon \in \mathcal{I}$.

A2 For $\epsilon \in \mathcal{I}$ the system (1) has a hyperbolic and asymptotically attracting limit cycle solution $\mathbf{x} = \gamma_\epsilon(t)$ with finite period T_ϵ, which we denote $\Gamma_\epsilon = \{\gamma_\epsilon(t), 0 \leq t \leq T_\epsilon\}$. We assume $\Gamma_\epsilon \subset \mathcal{D}$ for $\epsilon \in \mathcal{I}$.

A3 We assume that $0 \in \mathcal{I}$ and that the period can be written asymptotically for small ϵ as

$$T_\epsilon = T_0 + \epsilon T_1 + O(\epsilon^2), \tag{2}$$

where $0 < T_0 < \infty$ and $|T_1| < \infty$.

Note that the linear term T_1 is given by the well known formula

$$T_1 = -\int_0^{T_0} \mathbf{z}(t) \cdot \left.\frac{\partial\mathbf{F}(\gamma_0(t), \epsilon)}{\partial\epsilon}\right|_{\epsilon=0} dt, \tag{3}$$

where $\mathbf{z}(t) \in \mathbb{R}^n$ is the "infinitesimal phase response curve" (iPRC) of the limit cycle, see e.g. [20, 25]. The iPRC satisfies the adjoint equation with periodic boundary condition [6, 13]

$$\frac{d\mathbf{z}}{dt} = -D\mathbf{F}(\gamma_0(t), 0)^\intercal \mathbf{z}, \quad \mathbf{z}(t + T_0) = \mathbf{z}(t) \tag{4}$$

with the normalization condition

$$\mathbf{F}(\gamma_0(t), 0) \cdot \mathbf{z}(t) = 1. \tag{5}$$

We consider the homeostasis problem defined as follows. There exists a stable limit cycle solution $\mathbf{x} = \gamma_\epsilon(t)$ for (1) when $\epsilon \in \mathcal{I}$, with period T_ϵ. We denote the quantity of interest by q, and let $\mathcal{Q}$ represent the average of q evaluated around $\gamma_\epsilon(t)$ for one period, so that

$$\mathcal{Q} = \frac{1}{T_\epsilon}\int_0^{T_\epsilon} q(\gamma_\epsilon(t))\, dt. \tag{6}$$

We define a homeostasis criterion for limit-cycle systems in terms of the vanishing derivative of $\mathcal{Q}$ with respect to the control parameter, in analogy to the formulation by [10] for fixed-point systems:

Definition 1. *The average $\mathcal{Q}$ of a quantity q exhibits* infinitesimal homeostasis *at ϵ_0 if*

$$\left.\frac{\partial\mathcal{Q}}{\partial\epsilon}\right|_{\epsilon=\epsilon_0} = 0. \tag{7}$$

It has a simple homeostasis *point if further*

$$\left.\frac{\partial^2\mathcal{Q}}{\partial\epsilon^2}\right|_{\epsilon=\epsilon_0} \neq 0. \tag{8}$$

In the following, we provide a method to calculate $\partial\mathcal{Q}/\partial\epsilon$, allowing us to find homeostasis points for the mean value of a given quantity in a rhythmic control system. For stronger homeostasis conditions given by higher-order consecutive derivatives, such as chair homeostasis with zero first and second derivatives and nonvanishing third derivative [15], it becomes complicated for limit-cycle control systems and we do not discuss its analytical calculation here.

2.1 Infinitesimal shape response curve

The *infinitesimal shape response curve (iSRC)* introduced in [42] is a key tool in our homeostasis analysis. In this section we present a new, simplified derivation of the iSRC under the assumption that the underlying dynamical system is sufficiently smooth.

Fix a starting point $\mathbf{p}_0$ on the $\epsilon = 0$ limit cycle, and let $\mathcal{S}$ be a smooth Poincaré section transverse to the flow at $\mathbf{p}_0$. Standard results on the persistence of invariant manifolds under perturbation (cf. [44], §6.2) guarantee that for sufficiently small values of $|\epsilon|$, the perturbed limit cycle will intersect $\mathcal{S}$ at a smooth family of points

$$\mathbf{p}_\epsilon = \mathbf{p}_0 + \epsilon\mathbf{p}_1 + O(\epsilon^2). \tag{9}$$

Here $\mathbf{p}_0$ is the point where the limit cycle intersects $\mathcal{S}$, and $\mathbf{p}_1 \in \mathbb{R}^n$ is an element of the tangent space of $\mathcal{S}$ at $\mathbf{p}_0$. Let $\mathbf{x} = \gamma_\epsilon(t)$ be the limit cycle solution beginning at $\mathbf{p}_\epsilon$. Following Wang et al. [42] we write

$$\gamma_\epsilon(\tau_\epsilon(t)) = \gamma_0(t) + \epsilon\gamma_1(t) + O(\epsilon^2) \tag{10}$$

where $\tau_\epsilon(t)$ is a smooth, monotonically increasing function satisfying $\tau_\epsilon(0) = 0$ and $\tau_\epsilon(t+T_0) = \tau_\epsilon(t) + T_\epsilon$. One such rescaled time coordinate is given simply by the linear scaling:

$$\tau_\epsilon(t) = \frac{T_\epsilon}{T_0}t. \tag{11}$$

With time suitably rescaled to accommodate any change in the period of the limit cycle, the expansion (10) is uniform in time (cf. Lighthill's method of "strained coordinates" as discussed in [21] §6.3). The vector function $\gamma_1(t)$, periodic with period T_0, is defined as the infinitesimal shape response curve (iSRC). The iSRC quantifies the linearized change in the shape of the limit cycle trajectory Γ_ϵ upon a static perturbation of the parameter ϵ.

The authors of [42] define a nonhomogeneous variational equation for γ_1 with the linear time scaling (11):

$$\frac{d\gamma_1(t)}{dt} = D\mathbf{F}(\gamma_0(t),0)\gamma_1(t) + \nu_1\mathbf{F}(\gamma_0(t),0) + \left.\frac{\partial\mathbf{F}(\gamma_0(t),\epsilon)}{\partial\epsilon}\right|_{\epsilon=0}, \tag{12}$$

where $\nu_1 = \frac{T_1}{T_0}$ is independent of t. Here we generalize their equation into a nonuniform/local timing sensitivity case, for which we require an additional assumption:

A4 The functions $\gamma_\epsilon(t)$ and $\tau_\epsilon(t)$ must be continuously differentiable in both t and ϵ (cf. [A1]) for $\epsilon \in \mathcal{I}$.

The reasonableness of this assumption follows from the persistence of stable limit cycles under parametric perturbation, assumption [A3] concerning the period, and the use of a Poincaré section $\mathcal{S}$ to construct the intersection point $\mathbf{p}_\epsilon$, $\{\mathbf{p}_\epsilon\} = \mathcal{S}\cap\Gamma_\epsilon$, which sets $\gamma_\epsilon(0)$, and the possibility to specify the simple time rescaling (11).

We denote

$$\eta(t,\epsilon) = \frac{\partial\gamma_\epsilon(\tau_\epsilon(t))}{\partial\epsilon},$$

whence $\gamma_1(t) = \eta(t,0)$. Differentiating η with respect to t gives

$$\begin{aligned}\frac{\partial \eta(t,\epsilon)}{\partial t} &= \frac{\partial}{\partial t}\left(\frac{\partial \gamma_\epsilon(\tau_\epsilon(t))}{\partial \epsilon}\right) = \frac{\partial}{\partial \epsilon}\left(\frac{\partial \gamma_\epsilon(\tau_\epsilon(t))}{\partial t}\right) = \frac{\partial}{\partial \epsilon}\left(\mathbf{F}(\gamma_\epsilon(\tau_\epsilon(t)),\epsilon)\frac{\partial \tau_\epsilon(t)}{\partial t}\right) \\ &= \frac{\partial \mathbf{F}(\gamma_\epsilon(\tau_\epsilon(t)),\epsilon)}{\partial \epsilon}\frac{\partial \tau_\epsilon(t)}{\partial t} + \mathbf{F}(\gamma_\epsilon(\tau_\epsilon(t)),\epsilon)\frac{\partial}{\partial \epsilon}\left(\frac{\partial \tau_\epsilon(t)}{\partial t}\right) \\ &= \left(D\mathbf{F}(\gamma_\epsilon(\tau_\epsilon(t)),\epsilon)\eta(t,\epsilon) + \frac{\partial \mathbf{F}(\gamma_\epsilon(\tau_\epsilon(t)),\epsilon)}{\partial \epsilon}\right)\frac{\partial \tau_\epsilon(t)}{\partial t} + \mathbf{F}(\gamma_\epsilon(\tau_\epsilon(t)),\epsilon)\frac{\partial}{\partial \epsilon}\left(\frac{\partial \tau_\epsilon(t)}{\partial t}\right).\end{aligned}$$

Note that in the second step, changing the order of differentiation is allowed due to [A4]. Setting $\epsilon = 0$, we obtain a generalization of the infinitesimal SRC defined in [42], which is a T_0-periodic function satisfying a nonhomogeneous variational equation:

$$\frac{d\gamma_1(t)}{dt} = D\mathbf{F}(\gamma_0(t),0)\gamma_1(t) + \underbrace{\nu_1(t)\mathbf{F}(\gamma_0(t),0) + \left.\frac{\partial \mathbf{F}(\gamma_0(t),\epsilon)}{\partial \epsilon}\right|_{\epsilon=0}}_{\text{nonhomogeneous terms}}, \tag{13}$$

where $\nu_1(t) = \left.\frac{\partial^2 \tau_\epsilon(t)}{\partial \epsilon \partial t}\right|_{\epsilon=0}$ is a local timing sensitivity parameter. Compared with Theorem 1 in §9 of [5], the generalized iSRC system (13) has a T_0-periodic solution if and only if

$$\int_0^{T_0} \mathbf{z}(t) \cdot \left(\nu_1(t)\mathbf{F}(\gamma_0(t),0) + \left.\frac{\partial \mathbf{F}(\gamma_0(t),\epsilon)}{\partial \epsilon}\right|_{\epsilon=0}\right) dt = 0,$$

and so from (3) and (5),

$$\int_0^{T_0} \nu_1(t)\, dt = T_1. \tag{14}$$

In the special case of τ_ϵ with a constant slope (11), the generalized iSRC equation (13) reduces to (12), consistent with the formula obtained through a different argument by Wang et al. ~~in [42]~~. One can easily check that such choice of the rescaled time coordinate satisfies the condition (14) for a T_0-periodic solution. In the rest of the paper, we adopt this linear time rescaling and the corresponding iSRC equation (12).

Equation (12) requires an initial condition, which is

$$\gamma_1(0) = \mathbf{p}_1. \tag{15}$$

Changing the Poincaré section transverse to the unperturbed limit cycle, $\mathcal{S}$, changes the direction along which the base point $\mathbf{p}_\epsilon$ is displaced relative to $\mathbf{p}_0$. As shown in [42] and Lemma 1 below, the resulting iSRC functions are related by a simple phase shift (just as the asymptotic phase of an oscillator is itself only defined up to an additive constant). The iSRC is closely connected to the problem of tracking the change in any average quantity upon static perturbation of the limit cycle (changing ϵ), as we will show below.

2.2 Sensitivity of an average for limit cycle families

In this subsection we calculate how the average of any smooth quantity evaluated along a limit cycle trajectory changes as we vary a parameter influencing the limit cycle dynamics. We establish the connection between the iSRC and the average quantity, and we show that the sensitivity of the average is independent of our choice of Poincaré section, provided it is transverse to the limit cycle at the base point $\mathbf{p}_0$.

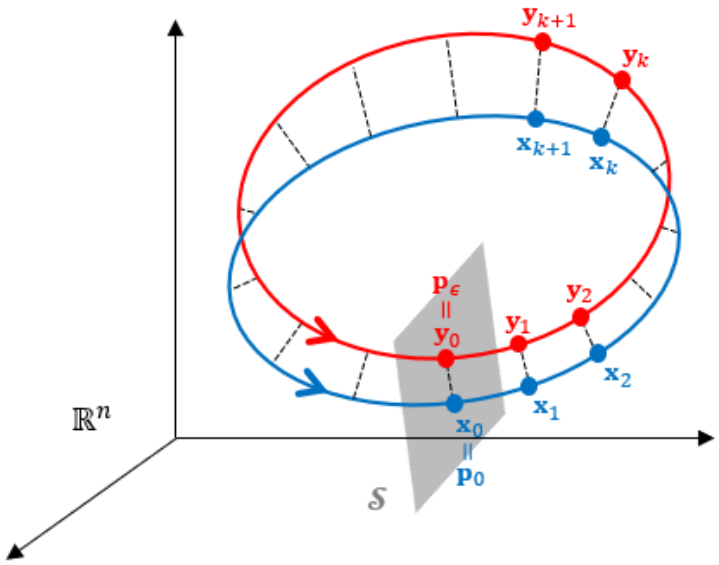

Figure 2: Two periodic orbits cut by a common Poincaré section, illustrating the construction for comparing the average of a quantity around each orbit. The section $\mathcal{S}$ intersects the loop $\mathbf{x}$ (blue trace) at point $\mathbf{x}_0 \equiv \mathbf{p}_0$. The section intersects the loop $\mathbf{y}$ (red trace) at point $\mathbf{y}_0 \equiv \mathbf{p}_\epsilon$. From the intersection point, each orbit is divided into n steps of equal time T_x/n or T_y/n, respectively, giving points $(\mathbf{x}_0, \mathbf{x}_1, \mathbf{x}_2, \ldots, \mathbf{x}_{n-1})$ (blue dots) and $(\mathbf{y}_0, \mathbf{y}_1, \mathbf{y}_2, \ldots, \mathbf{y}_{n-1})$ (red dots).

Suppose we have two periodic orbits, $\mathbf{x}$ and $\mathbf{y}$, with periods T_x and T_y, respectively. Fig. 2 illustrates a construction from which we can derive a comparison of the average of a quantity $q(\mathbf{x})$ around each orbit. As in the figure, mark off points of equal time, T_x/n or T_y/n, respectively. That is, define

$$\mathbf{x}_k = \mathbf{x}\left(\frac{k}{n}T_x\right), \quad \mathbf{y}_k = \mathbf{y}\left(\frac{k}{n}T_y\right)$$

Let $\mathcal{Q}_x$ be the average of a smooth function $q(\mathbf{x})$ around the trajectory $\mathbf{x}$, and similarly $\mathcal{Q}_y$. If q and the limit cycle are both smooth, then

$$\mathcal{Q}_x = \frac{1}{n}\sum_{k=0}^{n-1} q(\mathbf{x}_k) + O\left(\frac{1}{n^2}\right), \quad \text{as } n \to \infty,$$

with a similar expression for $\mathcal{Q}_y$. We want an expression for $\mathcal{Q}_y - \mathcal{Q}_x$ when $|\mathbf{p}_\epsilon - \mathbf{p}_0|$ is small.

Let γ_1 be the iSRC for a constant time rescaling function $\tau_\epsilon(t) = \frac{T_\epsilon}{T_0}t$, as defined above, and let $\mathbf{x}$ and $\mathbf{y}$ be the limit cycles generated by $\mathbf{F}(\cdot, 0)$ and $\mathbf{F}(\cdot, \epsilon)$, respectively. So $T_x = T_0$ and $T_y = T_\epsilon$. Then we have

$$\begin{aligned}
\mathcal{Q}_y - \mathcal{Q}_x &= \frac{1}{n}\sum_{k=0}^{n-1}(q(\mathbf{y}_k) - q(\mathbf{x}_k)) + O\left(\frac{1}{n^2}\right) \\
&= \frac{1}{n}\sum_{k=0}^{n-1}\nabla q(\mathbf{x}_k)\cdot(\mathbf{y}_k - \mathbf{x}_k) + O\left(|\mathbf{y}_k - \mathbf{x}_k|^2\right) + O\left(\frac{1}{n^2}\right) \\
&= \frac{\epsilon}{n}\sum_{k=0}^{n-1}\nabla q(\mathbf{x}_k)\cdot\gamma_1\left(\frac{k}{n}T_0\right) + O\left(\epsilon^2\right) + O\left(\frac{1}{n^2}\right).
\end{aligned}$$

The sensitivity of the average is

$$\frac{\partial \mathcal{Q}}{\partial \epsilon} = \lim_{\epsilon \to 0} \lim_{n \to \infty} \frac{\mathcal{Q}_y - \mathcal{Q}_x}{\epsilon} = \frac{1}{T_0} \int_0^{T_0} \nabla q(\gamma_0(t)) \cdot \gamma_1(t)\, dt. \tag{16}$$

Thus the change in the average value of any quantity around the limit cycle, when the limit cycle is changed due to a static (parametric) perturbation, is given by the infinitesimal shape response curve and the gradient of the quantity.

We show next that the sensitivity of the average quantity $\mathcal{Q}$ is invariant with respect to the choice of Poincaré section used to define the initial condition of the iSRC, $\gamma_1(0) = \mathbf{p}_1$. First, Lemma 1 and Fig. 3 show that the iSRC is a family of curves related by a phase shift. Lemma 1 previously appeared as Lemma 2.3 of [42], but the proof presented here is new and greatly simplified.

Lemma 1. *Under assumptions A1-A2, if $\eta(t)$ and $\xi(t)$ are solutions to the iSRC equation* (12) *with different Poincaré section, then*

$$\eta(t) - \xi(t) = \phi \mathbf{F}(\gamma_0(t), 0), \tag{17}$$

where $\phi \neq 0$ is the constant phase shift intoduced by the initial conditions $\eta(0) - \xi(0) = \phi \mathbf{F}(\gamma_0(0), 0)$.

Proof. Let

$$\Delta(t) = \eta(t) - \xi(t).$$

Then $\eta(t)$ and $\xi(t)$ satisfy the iSRC equation

$$\begin{aligned}
\frac{d\eta(t)}{dt} &= D\mathbf{F}(\gamma_0(t), 0)\eta(t) + \nu_1 \mathbf{F}(\gamma_0(t), 0) + \left.\frac{\partial \mathbf{F}(\gamma_0(t), \epsilon)}{\partial \epsilon}\right|_{\epsilon=0}, \\
\frac{d\xi(t)}{dt} &= D\mathbf{F}(\gamma_0(t), 0)\xi(t) + \nu_1 \mathbf{F}(\gamma_0(t), 0) + \left.\frac{\partial \mathbf{F}(\gamma_0(t), \epsilon)}{\partial \epsilon}\right|_{\epsilon=0},
\end{aligned}$$

with initial condition $\eta(0)$ and $\xi(0)$, respectively. Taking the difference of the above equations leads to

$$\frac{d\Delta(t)}{dt} = D\mathbf{F}(\gamma_0(t), 0)\Delta(t), \quad \Delta(0) = \eta(0) - \xi(0),$$

which has a unique solution

$$\Delta(t) = \phi \mathbf{F}(\gamma_0(t), 0)$$

with ϕ given by $\eta(0) - \xi(0) = \phi \mathbf{F}(\gamma_0(0), 0)$. □

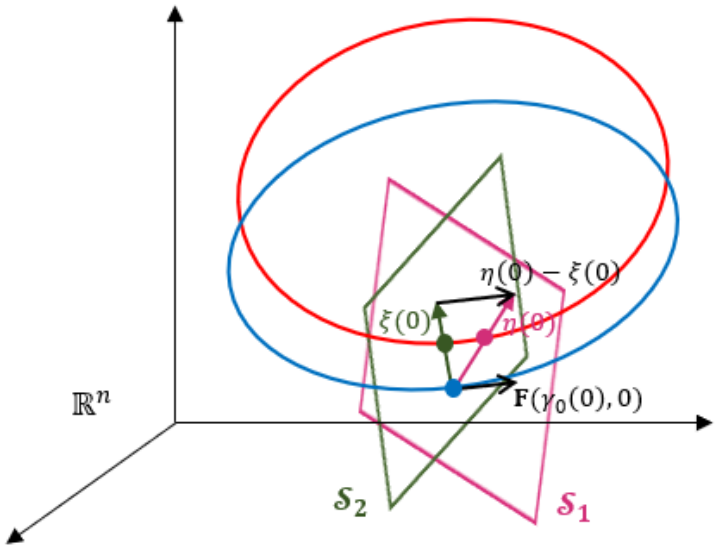

Figure 3: Two distinct iSRCs differ along the unperturbed flow (see Lemma 1). The unperturbed limit cycle (blue trace) intersects sections $\mathcal{S}_1$ and $\mathcal{S}_2$ at $\mathbf{p}_0 = \gamma_0(0)$ (blue dot). The perturbed limit cycle (red trace) intersects $\mathcal{S}_1$ at $\mathbf{p}_\epsilon^1$ (magenta dot) and intersects $\mathcal{S}_2$ at $\mathbf{p}_\epsilon^2$ (green dot). Magenta arrow shows the direction of the linear shape displacement $\eta(0) = \mathbf{p}_1^1 = \lim_{\epsilon=0} \frac{\mathbf{p}_\epsilon^1 - \mathbf{p}_0}{\epsilon}$; green arrow shows the direction of the linear shape displacement $\xi(0) = \mathbf{p}_1^2 = \lim_{\epsilon=0} \frac{\mathbf{p}_\epsilon^2 - \mathbf{p}_0}{\epsilon}$ (cf. (9)). Their difference is parallel with the unperturbed vector field at $\gamma_0(0)$. For further shape responses as time evolves, $\eta(t)$ and $\xi(t)$ always differ along the direction of $\gamma_0(t)$ (not shown).

By eq. (16), the sensitivity of the average given by different shape response curves follows

$$\begin{aligned}\left(\frac{\partial \mathcal{Q}}{\partial \epsilon}\right)_\eta - \left(\frac{\partial \mathcal{Q}}{\partial \epsilon}\right)_\xi &= \frac{1}{T_0}\int_0^{T_0} \nabla q(\gamma_0(t)) \cdot \eta(t)\, dt - \frac{1}{T_0}\int_0^{T_0} \nabla q(\gamma_0(t)) \cdot \xi(t)\, dt \\ &= \frac{1}{T_0}\int_0^{T_0} \nabla q(\gamma_0(t)) \cdot \Delta(t)\, dt. \end{aligned} \tag{18}$$

Then, from the periodicity of $\gamma_0(t)$, fundamental theorem of calculus, eq. (1) and Lemma 1,

$$\begin{aligned} 0 &= q(\gamma_0(T_0)) - q(\gamma_0(0)) \\ &= \int_0^{T_0} \frac{d}{dt}\left(q(\gamma_0(t))\right)\, dt = \int_0^{T_0} \nabla q(\gamma_0(t)) \cdot \frac{d\gamma_0(t)}{dt}\, dt \\ &= \int_0^{T_0} \nabla q(\gamma_0(t)) \cdot \mathbf{F}(\gamma_0(t),0)\, dt = \frac{1}{\phi}\int_0^{T_0} \nabla q(\gamma_0(t)) \cdot \Delta(t)\, dt, \end{aligned}$$

which gives

$$\left(\frac{\partial \mathcal{Q}}{\partial \epsilon}\right)_\eta = \left(\frac{\partial \mathcal{Q}}{\partial \epsilon}\right)_\xi. \tag{19}$$

Thus, the sensitivity of an average is independent of the choice of the Poincaré section.

3 Applications

In this section, to illustrate the principles derived above, we consider two specific smooth systems: the well-known Hodgkin-Huxley model of excitability in the squid giant axon, which

exhibits large-amplitude limit cycles, (cf. [20], §2.3), and a metabolic feedforward-regulatory structure studied in [11], which exhibits small-amplitude oscillations. For each application, we find its infinitesimal shape response curves and illustrate the empirical curves of the average with analytically derived tangent curves for quantities of interest. Specifically, in the Hodgkin-Huxley example, we illustrate some basic principles and calculation related to the iSRC described above; for the feedforward chain, we illustrate the utility of our rate of change formula to study homeostasis behavior of some averaged quantity. Simulation codes required to produce each figure are available at https://github.com/zhuojunyu-appliedmath/Homeostasis-iSRC.

3.1 Hodgkin-Huxley model

In this subsection, we use the Hodgkin-Huxley model ([20], §2.3) to illustrate how to compute the shape response curve, the relation between different components in the iSRC family, and its application to compute the sensitivity of the average of some physical quantities, which is independent of the choice of the iSRC.

The 4-dimensional Hodgkin-Huxley system is

$$\begin{aligned} C\dot{V} &= I - g_{\mathrm{K}} n^4 (V - E_{\mathrm{K}}) - g_{\mathrm{Na}} m^3 h (V - E_{\mathrm{Na}}) - g_{\mathrm{L}} (V - E_{\mathrm{L}}) \\ \dot{n} &= \alpha_n(V)(1-n) - \beta_n(V) n \\ \dot{m} &= \alpha_m(V)(1-m) - \beta_m(V) m \\ \dot{h} &= \alpha_h(V)(1-h) - \beta_h(V) h. \end{aligned} \tag{20}$$

Parameters and the activation/inactivation rate functions α_x, β_x are given in Appendix A. We apply a small static perturbation to the injected current, $I \to I + \epsilon$, and rescale the timing of the perturbed trajectory by $\tau_\epsilon(t) = \frac{T_\epsilon}{T_0} t$. As a reference, Fig. 4 shows the time course of the model for two different values of the applied current, each plotted for three periods.

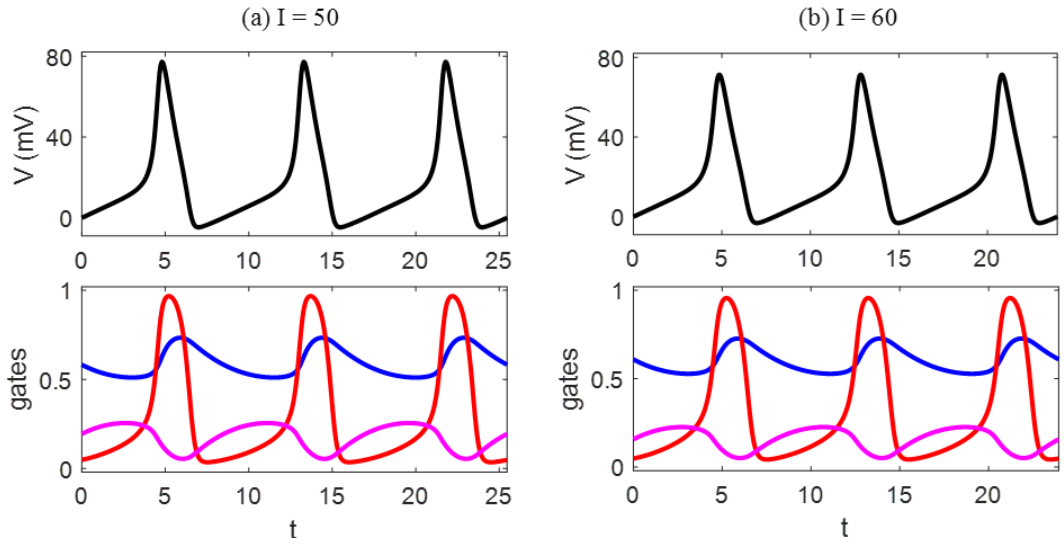

Figure 4: A reference figure showing V (black curve), n (blue curve), m (red curve), h (magenta curve) for two different values of the current, $I = 50$ (left) and $I = 60$ (right), with period $T_{I=50} = 8.49$ and $T_{I=60} = 7.98$, respectively.

We compute two solutions to the iSRC equation (12), with different Poincaré sections, for $I = 50$, and compare their difference with the flow of the unperturbed limit cycle. Define a

Poincaré section

$$\mathcal{S}_1 = \left\{ V = 0,\ \frac{dV}{dt} > 0 \right\}.$$

This section intersects the unperturbed limit cycle at point $\mathbf{p}_0 = (0, n_0, m_0, h_0)$ and intersects the perturbed limit cycle at point $\mathbf{p}_\epsilon^1$. As in (9), the linear displacement from $\mathbf{p}_0$ is

$$\mathbf{p}_1^1 = \lim_{\epsilon=0} \frac{\mathbf{p}_\epsilon^1 - \mathbf{p}_0}{\epsilon} = \left(0,\ \left.\frac{\partial n}{\partial \epsilon}\right|_{V=0},\ \left.\frac{\partial m}{\partial \epsilon}\right|_{V=0},\ \left.\frac{\partial h}{\partial \epsilon}\right|_{V=0} \right)\Bigg|_{\epsilon=0}.$$

Take another Poincaré section transverse to the unperturbed limit cycle at the same base point $\mathbf{p}_0$:

$$\mathcal{S}_2 = \left\{ n = n_0,\ \frac{dn}{dt} < 0 \right\},$$

which intersects the perturbed flow at $\mathbf{p}_\epsilon^2$.Then,

$$\mathbf{p}_1^2 = \lim_{\epsilon=0} \frac{\mathbf{p}_\epsilon^2 - \mathbf{p}_0}{\epsilon} = \left(\left.\frac{\partial V}{\partial \epsilon}\right|_{n=n_0},\ 0,\ \left.\frac{\partial m}{\partial \epsilon}\right|_{n=n_0},\ \left.\frac{\partial h}{\partial \epsilon}\right|_{n=n_0} \right)\Bigg|_{\epsilon=0}.$$

Numerically, we approximate $\mathbf{p}_1^i\ (i = 1, 2)$ by $\mathbf{p}_1^i \approx (\mathbf{p}_\epsilon^i - \mathbf{p}_0)/\epsilon$ with $\epsilon = 0.5$. Let $\eta(t)$ be a representative T_0-periodic iSRC given by the initial condition $\eta(0) = \mathbf{p}_1^1$ (cf. (15)) and $\xi(t)$ be another T_0-periodic iSRC with $\xi(0) = \mathbf{p}_1^2$. Fig. 5 shows the components of $\eta(t)$ and $\xi(t)$ to illustrate how the shape changes in response to the perturbation. Note that changing the direction of the Poincaré section through the common base point $\mathbf{p}_0$ significantly changes each component of the iSRC.

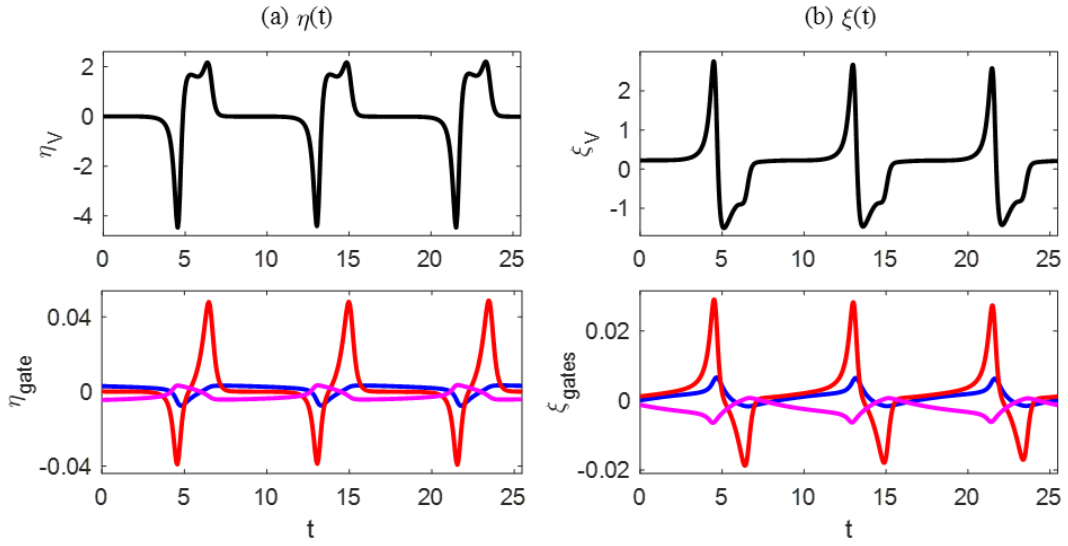

Figure 5: ISRC components of four variables of the Hodgkin-Huxley system, for two different Poincaré sections / initial conditions. **(a)**: The iSRC $\eta(t)$ specified by section $\mathcal{S}_1$. **(b)**: The iSRC $\xi(t)$ specified by $\mathcal{S}_2$. Colors as in Fig. 4. Each case has the same reference trajectory with driving current $I = 50$ and period $T_0 = 8.49$.

As stated in Lemma 1, despite different shape response curves shown in Fig. 5, they are related by a fixed offset — a vector in the direction of the flow along the unperturbed limit cycle, represented by a constant phase shift. In our example, we have $\phi \approx -0.0585$ and Fig. 6

illustrates that their difference $\Delta(t)$ shows great agreement with $\phi\mathbf{F}(\gamma_0(t), 0)$, as proof of the concept.

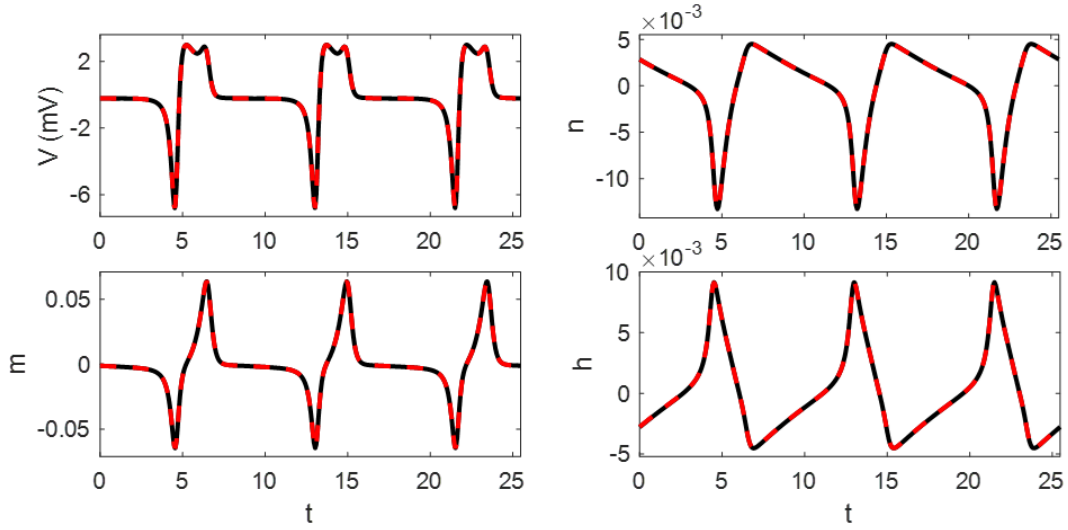

Figure 6: Difference of the two iSRCs in the four directions. Black solid trace: $\eta(t) - \xi(t)$; red dashed trace: $\phi\mathbf{F}(\gamma_0(t), 0)$ with $\phi = -0.0585$. The curves show excellent agreement.

To demonstrate the utility of the shape response curve for determining the sensitivity of an arbitrary quantity as a control parameter is varied, we focus on the average of three quantities — membrane potential, sodium current and potassium current — as we vary the value of the injected current. The expressions of the two currents are

$$I_{\mathrm{Na}} = -g_{\mathrm{Na}} m^3 h (V - E_{\mathrm{Na}}), \qquad I_{\mathrm{K}} = -g_{\mathrm{K}} n^4 (V - E_{\mathrm{K}}).$$

We show that the slope analytically derived from the rate of change formula (16) is in line with the average curve. For instance, Fig. 7 illustrates the case evaluated at $I = 50$, with $\eta(t)$ chosen from the iSRC family.

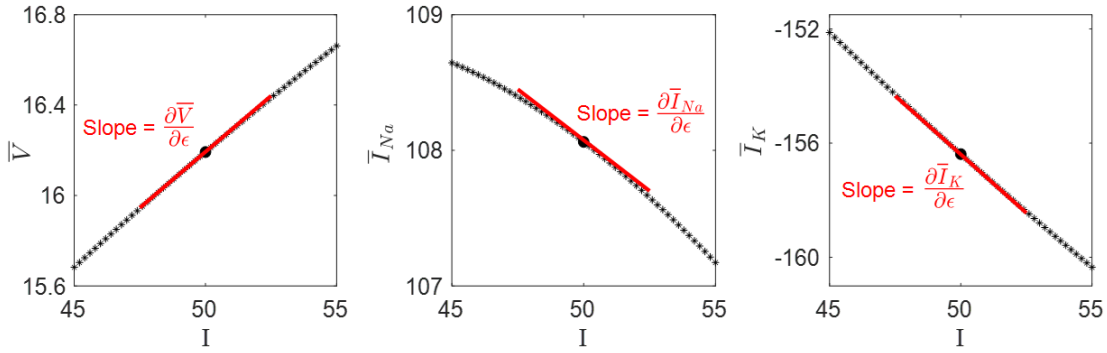

Figure 7: Empirical curves with analytically derived tangent curves for voltage V (left), sodium current I_{Na} (middle) and potassium current I_{K} (right). Black star: direct calculation of the average of the three quantities as the value of I varies. Red solid: tangent line at $I = 50$ with slope analytically derived from the iSRC calculation with $\eta(t)$ chosen, i.e., $\mathcal{Q} = \mathcal{Q}_{I=50} + \frac{\partial \mathcal{Q}}{\partial \epsilon}\big|_{I=50} \cdot (I - 50)$.

As expected from our theory, the average of any quantity is an invariant with respect to which element of the family is selected by the Poincaré section defining the initial conditions.

The slopes at $I = 50$ given by $\eta(t)$ (cf. Fig. 7) are

$$\left(\frac{\partial \overline{V}}{\partial \epsilon}\right)_{\eta} = 0.099187, \quad \left(\frac{\partial \overline{I}_{\mathrm{Na}}}{\partial \epsilon}\right)_{\eta} = -0.148480, \quad \left(\frac{\partial \overline{I}_{\mathrm{K}}}{\partial \epsilon}\right)_{\eta} = -0.821531.$$

If calculated by $\xi(t)$, the results are

$$\left(\frac{\partial \overline{V}}{\partial \epsilon}\right)_{\xi} = 0.099161, \quad \left(\frac{\partial \overline{I}_{\mathrm{Na}}}{\partial \epsilon}\right)_{\xi} = -0.150017, \quad \left(\frac{\partial \overline{I}_{\mathrm{K}}}{\partial \epsilon}\right)_{\xi} = -0.820998,$$

within 1.04% error relative to those calculated by $\eta(t)$.

3.2 Feedforward network

Duncan et al. [10, 11] investigated homeostasis in the presence of Hopf bifurcations in several metabolic networks supporting limit cycle oscillations with a wide range of near-constant amplitudes and periods. They showed that when the amplitudes of the oscillations are relatively small, the output variable remains near a homeostatic plateau. We adopt one of their examples and apply our method to illustrate homeostasis for limit cycles in the sense of averaging.

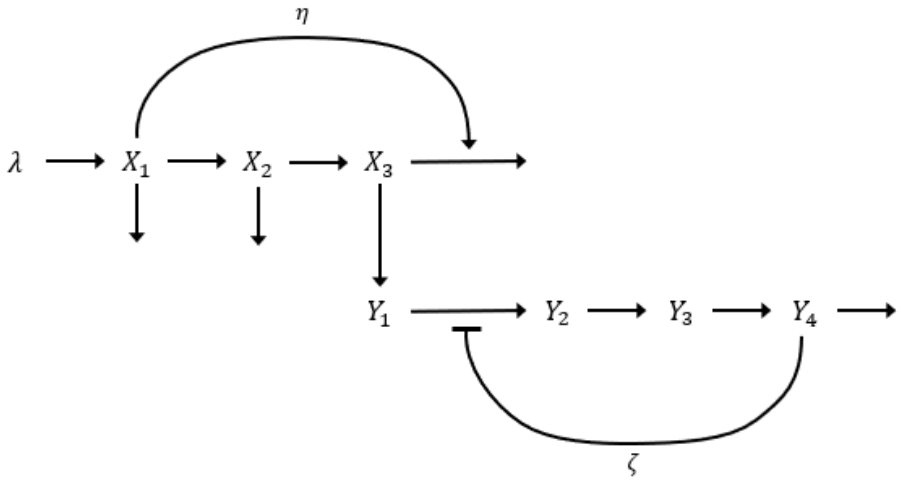

Figure 8: A simple metabolic chain exhibiting the coexistence of homeostasis-Hopf-bifurcation, redrawn from [11]. λ is the input parameter to the network. X_3 has a homeostasis point and acts as an input to the Y system which undergoes a Hopf bifurcation.

Fig. 8 shows a feedforward network studied in [11]. The equations for the system are

$$\begin{aligned}
\dot{x_1} &= \lambda - 2x_1 \\
\dot{x_2} &= x_1 - 2x_2 \\
\dot{x_3} &= x_2 - (1 + \eta(x_1))x_3 \\
\dot{y_1} &= x_3 - \zeta(y_4)y_1 \\
\dot{y_2} &= \zeta(y_4)y_1 - y_2 \\
\dot{y_3} &= y_2 - y_3 \\
\dot{y_4} &= y_3 - y_4
\end{aligned} \tag{21}$$

where λ is the input parameter and y_4 is considered as the output variable. There are two saturating nonlinearities taking the forms $\eta(x) = 1/(1 + \exp\left[\frac{c-x}{a}\right])$ and $\zeta(y) = 10/(1 +$

$y^{10}) + b$. The qualitative behaviors of the system can be distinct under different choices from the parameter space $\{a,\, b,\, c\}$, and [11] listed all possible varieties. We choose two cases — $(a,\, b,\, c) = (0.73,\, 0.01,\, 4.78)$ and $(a,\, b,\, c) = (0.65,\, 0.01,\, 4.88)$ (cf. [11], Fig. 9(d,g)) to study the homeostasis of averages of the system.

For any $\lambda \in [5, 15]$, the X system always approaches a stable fixed point and X_3 feeds into the Y network which can maintain small-amplitude oscillations in some range of λ. In Fig. 9, we offer a reference figure showing the oscillations of variable y_4 at $\lambda = 10.5$ for case 1 and at $\lambda = 10$ for case 2, and their respective infinitesimal shape response curve $\eta(t)$ in the y_4 direction, specified by Poincaré section $\{y_4 = 1.6,\, \frac{dy_4}{dt} > 0\}$. In the first case, the y_4 component of η has a symmetric area above and below the horizontal axis for each period. Following formula (16) and Definition 1, the average of y_4 at $\lambda = 10.5$ is an infinitesimal homeostasis point:

$$\begin{aligned} \frac{\partial \overline{y}_4}{\partial \lambda}\bigg|_{\lambda=10.5} &= \frac{1}{T_0}\int_0^{T_0} [0,\, \cdots,\, 0,\, 1]^{\mathsf{T}} \cdot \eta(t)\, dt \\ &= \frac{1}{T_0}\int_0^{T_0} \eta_{y_4}(t)\, dt = 0. \end{aligned}$$

Likewise, in the second case, the location of its iSRC indicates a negative sensitivity of $\overline{y}_4$ at $\lambda = 10$. For the behavior of y_4 over other values of λ, we give more details in what follows.

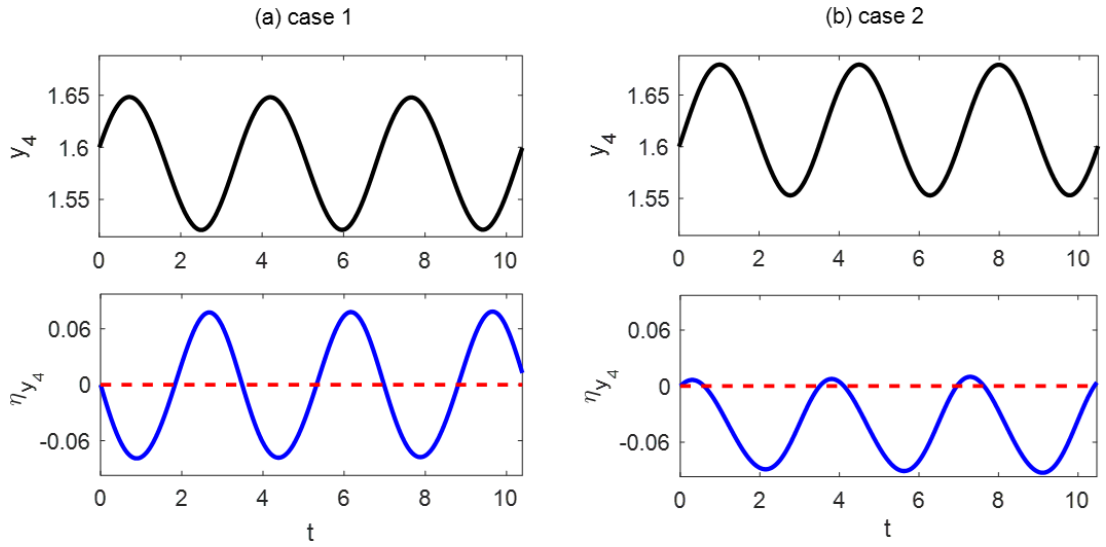

Figure 9: A reference figure showing the time evolution of y_4 (top panels) at $\lambda = 10.5$ for case 1 (left) and at $\lambda = 10$ for case 2 (right) and their respective iSRC in the y_4 component, defined by the section $\{y_4 = 1.6,\, \frac{dy_4}{dt} > 0\}$ (bottom panels). The curves are plotted using the same scale for the vertical axes. **(a)** case 1: $a = 0.73$, $b = 0.01$, $c = 4.78$, with period $T_0 = 3.46$. The compensating area of $\eta_{y_4}(t)$ above and below $\eta_{y_4} \equiv 0$ indicates $\frac{\partial \overline{y}_4}{\partial \lambda}\big|_{\lambda=10.5} = 0$. **(b)** case 2: $a = 0.65$, $b = 0.01$, $c = 4.88$, with period $T_0 = 3.49$. The iSRC η_{y_4} is mostly located below the zero horizontal axis, leading to a negative λ-derivative of $\overline{y}_4$ at $\lambda = 10$. Compare Fig. 10.

We apply the averaging method stated above to study the behavior of quantity $w \equiv y_4$, in terms of the *stable* critical element, for the two cases over $\lambda \in [5, 15]$. In the ranges of λ in which the equilibrium point is stable (blue curves in Fig. 10, top panels), we can directly solve (21) for the steady state condition to obtain the output value w as a function of the input

parameter λ at steady-state:

$$w(\lambda) = \frac{\lambda}{4}\left(\frac{1}{1+\eta\left(\frac{\lambda}{2}\right)}\right),$$

from which the first λ-derivative of w can be computed directly —

$$\frac{dw}{d\lambda} = \frac{2a\left(1+\eta\left(\frac{\lambda}{2}\right)\right) - \lambda e^{\frac{2c-\lambda}{2a}}\eta\left(\frac{\lambda}{2}\right)^2}{8a\left(1+\eta\left(\frac{\lambda}{2}\right)\right)^2}.$$

~~For the ranges of λ in which the equilibrium point is stable (blue curves in Fig. 10, top panels),~~ This calculation allows us to look for homeostasis points such that $dw/d\lambda = 0$. Note that in regions where the fixed point is unstable and gives way to a stable limit cycle, the unstable equilibrium also follows the same λ-derivative formula, but we are not concerned with its behavior. Instead, we seek the *average* output value $\overline{w}$ around the stable limit cycle, and we can apply our shape response curve method to find the sensitivity of ~~the *average* output value~~ $\overline{w}$, see (16). We repeat here the analytical calculation of $d\overline{w}/d\lambda$ for any value of $\lambda \in [5, 15]$ ($\overline{w}$ reduces to w when it is a stable equilibrium which has "period zero"):

$$\frac{d\overline{w}}{d\lambda} = \begin{cases} \frac{2a\left(1+\eta\left(\frac{\lambda}{2}\right)\right) - \lambda e^{\frac{2c-\lambda}{2a}}\eta\left(\frac{\lambda}{2}\right)^2}{8a\left(1+\eta\left(\frac{\lambda}{2}\right)\right)^2}, & \lambda \in \{\text{range for stable equilibra}\} \\ \frac{1}{T_0(\lambda)}\int_0^{T_0(\lambda)} \nabla z(\gamma_0(t)) \cdot \gamma_1(t)\, dt, & \lambda \in \{\text{range for stable limit cycles}\} \end{cases} \tag{22}$$

where $\gamma_0(t)$ is the limit cycle solution at a given λ with period $T_0(\lambda)$ and $\gamma_1(t)$ is the solution to the iSRC equation (12).

We obtain excellent agreement between the analytical result and direct numerical differentiation of the average curve, see Fig. 10. In the first case, the top panel shows that for small values of λ, the equilibria of y_4 are stable and change rapidly (blue curve). The equilibrium loses stability via a supercritical Hopf bifurcation (magenta dot) and gives birth to small-size limit cycle attractors with the amplitudes shown by green curves. The coexisting unstable fixed points are represented with a red curve. When λ is large, the oscillatory behavior of y_4 stops and the unstable equilibrium regains stability via another Hopf bifurcation. In the middle panel, we show the average of y_4. For the ranges of λ without oscillations, it is simply viewed as the equilibria of y_4, $\overline{y}_4 = y_4$ (blue curve); otherwise, it is integrated around the limit cycle, $\overline{y}_4 = \frac{1}{T_0}\int_0^{T_0} y_4(\gamma_0(t))\, dt$ (red curve). At bottom, the analytical calculation of $\partial\overline{y}_4/\partial\lambda$, following (22), is shown by solid curves, which shows good agreement with the direct calculation of the slope of $\overline{y}_4$ (green dashed curve). By Definition 1, the averages evaluated along the limit cycles are homeostatic for intermediate values of the input with two simple homeostasis points (grey dot). For case 2, we follow the same method and again demonstrate the accuracy of our formula for calculating the sensitivity of the averaged quantity. For stable limit-cycle control systems, this indicates that the shape response curve for determining the sensitivity of the average output can be a reliable tool to study limit-cycle homeostasis.

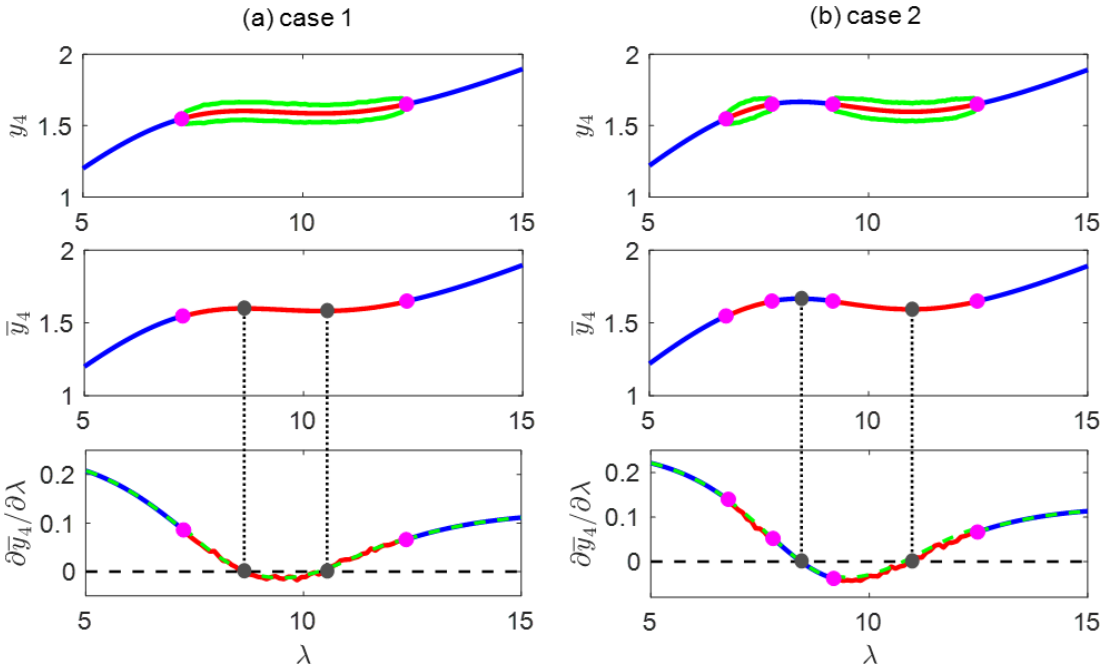

Figure 10: Behavior of the output variable Y_4 as the input λ varies in the chain network. **(a)** case 1: $a = 0.73$, $b = 0.01$, $c = 4.78$; **(b)** case 2: $a = 0.65$, $b = 0.01$, $c = 4.88$. **Top panels:** the value of y_4 at equilibrium. Hopf bifurcation points are marked in magenta dots. For small λ, the equilibria are stable (blue trace); at the bifurcation point, the equilibrium becomes unstable (red trace) and coexists with a stable limit cycle. The maximum and minimum values of the limit cycles are shown in green curves. At next Hopf point, the oscillations terminate and the equilibrium regains stability. (Cf. Fig. 9(d,g) from [11].) **Middle panels:** the average of y_4. In the limit-cycle region, it is evaluated along the limit cycle (red trace). In the interval for stable equilibria, the average is simply the equilibrium itself (blue trace). **Bottom panels:** the analytically and numerically determined λ-derivative of $\overline{y}_4$. Solid trace: analytical calculation given by eq. (22). Dashed green trace: direct numerical differentiation of the average curve in the middle panel. The points where $\partial\overline{y}_4/\partial\lambda = 0$ (grey dots) match well with those with zero slope in the middle panels, which indicates simple homeostasis averages for the limit cycles.

4 Discussion

Biological homeostasis requires that a quantity of interest – given by an "output" z – maintains an approximately constant value as the external conditions – given by an "input" λ – vary. This notion is widely considered in the networks of "*admissible vector fields*", which associates a state variable with each node and associates coupling terms between these node variables with the arrows of the network [15]. In this context, *input-output networks* are constructed, with only one distinguished input node depending on the input parameter(s) and one different distinguished output node. For the output node, there are many observables given by the time series of its corresponding state variable. A natural observable is the *equilibrium* of the output variable. Golubitsky and coauthors define an *input-output function* that maps the input parameter to the equilibrium, and have conducted a comprehensive study on the homeostasis in terms of the equilibrium points [10, 11, 15, 16, 17, 22, 34, 43].

The infinitesimal notion of homeostasis (namely, the derivative of the input–output function is vanishing at an isolated point) is developed to introduce singularity theory into the anal-

ysis of homeostasis properties of biological systems [15]. ~~The mathematical formulation of infinitesimal homeostasis allows the application of singularity theory to analyze homeostasis properties of biological systems.~~ Specifically, Golubitsky and Stewart use normal form theory to discuss universal unfoldings of singularities associated with homeostasis, distinguishing *simple homeostasis* (when $dz/d\lambda = 0$ and $d^2z/d\lambda^2 \neq 0$; in this case the normal form is $z(\lambda) = \pm\lambda^2$) from *chair homeostasis* (when $dz/d\lambda = 0$ and $d^2z/d\lambda^2 = 0$ but $d^3z/d\lambda^3 \neq 0$; in this case the normal form is $z(\lambda) = \pm\lambda^3$ and the universal unfolding is $z(\lambda) = \pm\lambda^3 + a\lambda$). Transformation of a homeostasis point to a normal form representation allows them to introduce the notion of a *δ-homeostasis region*, i.e. the set of λ such that $z(\lambda)$ remains within $\pm\delta$ of the homeostasis value. This notion provides a quantitative basis for comparing the robustness of different homeostasis mechanisms.

In addition, Golubitsky and Stewart characterize a reasonable class of coordinate changes under which homeostasis of a given variable is preserved. They also develop a linear-algebraic method (by a straightforward application of Cramer's rule) for finding homeostasis points in a given model, and identify mechanisms giving rise to homeostasis in specific networks, such as feed-forward (or lateral) inhibition. In subsequent work Golubitsky and Wang [17] ~~classified all homeostatic mechanisms in a family of small networks~~ give a classification of "homeostasis types" in three-node input–output networks, which is then generalized into arbitrarily large input–output networks [43].

We observe that all of this analysis is premised on being able to discuss the derivative $dz/d\lambda$. In many rhythmic physiological systems, however, homeostasis is maintained through control of limit cycles rather than equilibrium points. A special observable for this paper is the *average* of a quantity of interest, or an output, taken around the limit cycle, and the main contribution is to introduce a way to calculate the derivative of the average with respect to the input parameter. ~~The main contribution of this paper is to introduce a way to calculate the derivative $d\mathcal{Q}/d\lambda$ for a quantity of interest q averaged over a limit cycle.~~ This opens the possibility of analyzing factors contributing to homeostasis, such as sensory feedback [24, 45], in physiological systems operating with large amplitude limit cycles, as in breathing, heartbeat, locomotion, feeding, and other vital behaviors. Thus this paper takes a first step towards a theory for homeostasis for systems in which the locus of control is a limit cycle rather than a fixed point.

We follow the concepts of homeostasis points defined by Golubitsky and Stewart related to fixed-point systems and build a homeostasis criterion for smooth limit-cycle control systems in terms of the vanishing derivative of $\bar{z}$ with respect to λ. We provide a formula for analytically calculating the first order λ-derivative of $\bar{z}$. (In fact, when the limit cycle case has "period zero" the formula reduces to the much simpler formula for the equilibrium case in terms of Cramer's rule given by [15, 22].) At some point λ_0 where $\bar{z}'(\lambda_0) = 0$, one can easily tell whether the second derivative vanishes through calculating the first derivative over a small neighborhood of λ_0, so that a simple homeostasis point can be distinguished. We applied such a method to the metabolic regulatory network discussed in §3.2. This opens up an approach to examine simple homeostasis behavior of maintaining near-constant averaged quantities around limit cycles. Chair points, a more robust form of homeostasis, require judgment of all derivatives up to the third order, complicating the analysis for limit cycle systems, which is beyond the scope of the present paper.

Our rate of change formula is based on the infinitesimal shape response curve developed by Wang et al. [42]. The iSRC, a family of curves parameterized by a simple phase shift, quantifies the linearized change in the *shape* of a periodic orbit in response to a sustained perturbation. The accuracy of the iSRC depends on its local timing sensitivity induced by the timing response of the system to the perturbation, and [42] chose a linear time change in their formulation. We rederive the iSRC equation with a simplified approach and present a generalization of the

equation to any arbitrary rescaled time coordinate (see eq. (13)). Despite the phase-shift ambiguity of the iSRC, we show that the sensitivity of the average is invariant with respect to which element of the iSRC family is selected by the Poincaré section defining the initial conditions. This observation is consistent with physical intuition but is nevertheless important to establish mathematically. All the theoretical principles related to the iSRC are well verified in the Hodgkin-Huxley example discussed in §3.1.

A recent theory for a complete classification of "homeostasis types" regarding the input-output network with an equilibrium path is developed by Wang et al. [17, 43]. The *homeostasis matrix*, whose entries are linearized couplings between nodes, plays a key role in finding equilibrium homeostasis points. They factor the determinant polynomial of the homeostasis matrix, and introduce four different types of possible homeostasis associated with different structures of the network. Specifically, each factor corresponds to a subnetwork of the input-output network. In contrast, in limit-cycle systems, such a structural classification remains elusive. To see why, consider our analysis of an input-output network (e.g., §3.2). Here, when we average terms around the output limit cycle, our derivative formula (16) involves integral and shape response curves which cannot immediately be related algebraically to the network architecture. Extending the classification theory would be an interesting future direction.

Finally, we note that although here we only consider the homeostasis condition for limit cycle systems arising from a smooth vector field, the iSRC analysis of [42] encompasses certain classes of *nonsmooth* dynamical systems that are important in motor control. For example, one finds limit cycles for which the trajectory passes through a switching surface across which the vector field changes discontinuously [33, 39], as well as "limit cycle with sliding component" systems [42], in which the trajectory is confined to a constraint surface for part of the period. In locomotion problems these nonsmooth dynamics typically appear in the transition between a "power stroke" and "recovery stroke" in a repeated motion, such as swing/stance transitions in walking [41], scratching [40], inspiration/expiration transitions in breathing [9, 27, 28], and flexing/extending transitions in grasping or pulling movements [26, 38]. Although we do not pursue these nonsmooth examples here, we do not foresee any fundamental difficulty applying our sensitivity-of-the-average formula (16) to these cases.

5 Acknowledgments

PT thanks the Oberlin College Department of Mathematics for research support.

A Hodgkin-Huxley Equations

In the Hodgkin-Huxley system (20), the activation/inactivation rate functions are

$$\alpha_n(V) = 0.01\frac{10-V}{\exp\left(\frac{10-V}{10}\right)-1}, \qquad \beta_n(V) = 0.125\exp\left(\frac{-V}{80}\right),$$
$$\alpha_m(V) = 0.1\frac{25-V}{\exp\left(\frac{25-V}{10}\right)-1}, \qquad \beta_m(V) = 4\exp\left(\frac{-V}{18}\right),$$
$$\alpha_h(V) = 0.07\exp\left(\frac{-V}{20}\right), \qquad \beta_h(V) = \frac{1}{\exp\left(\frac{30-V}{10}\right)+1}.$$

Parameter values for the system are listed in Table 1.

Table 1: Parameter values for HH system

Conductances (mS/cm^2)	Reversal potentials (mV)	Other
$g_{\text{L}} = 0.3$	$E_{\text{L}} = 10.6$	$C = 1\ \mu\text{F/cm}^2$
$g_{\text{K}} = 36$	$E_{\text{K}} = -12$	I as in figure
$g_{\text{Na}} = 120$	$E_{\text{Na}} = 120$	

B Declarations

B.1 Funding

This work was supported in part by National Institutes of Health BRAIN Initiative grant R01 NS118606, and NSF grant DMS-2052109.

B.2 Conflicts of interest/Competing interests

The authors declare no competing interests.

B.3 Availability of data and material (data transparency)

Not applicable.

B.4 Code availability (software application or custom code)

Custom code written in Matlab is available at
`https://github.com/zhuojunyu-appliedmath/Homeostasis-iSRC`.

B.5 Authors' contributions

ZY and PJT designed the study. ZY and PJT derived the results. ZY performed the simulations. ZY and PJT wrote the manuscript.

References

[1] Jooeun Ahn and Neville Hogan. A simple state-determined model reproduces entrainment and phase-locking of human walking. *PloS one*, 7(11):e47963, 2012.

[2] Fernando Antoneli, Martin Golubitsky, and Ian Stewart. Homeostasis in a feed forward loop gene regulatory motif. *Journal of Theoretical Biology*, 445:103–109, 2018.

[3] Shinya Aoi and Kazuo Tsuchiya. Locomotion control of a biped robot using nonlinear oscillators. *Autonomous robots*, 19(3):219–232, 2005.

[4] Claude Bernard. *Leçons sur les phénomènes de la vie commune aux animaux et aux végétaux*, volume 1. Baillière, Paris, 1878.

[5] Roger W Brockett. *Finite dimensional linear systems*. SIAM, 2015.

[6] Eric Brown, Jeff Moehlis, and Philip Holmes. On the phase reduction and response dynamics of neural oscillator populations. *Neural computation*, 16(4):673–715, 2004.

[7] Eugene N. Bruce. Nonlinear dynamics of respiratory reflexes. *IFAC Proceedings Volumes*, 27(1):497–500, 1994.

[8] Walter B Cannon. Organization for physiological homeostasis. *Physiological reviews*, 9(3):399–431, 1929.

[9] Casey O Diekman, Peter J Thomas, and Christopher G Wilson. Eupnea, tachypnea, and autoresuscitation in a closed-loop respiratory control model. *Journal of neurophysiology*, 118(4):2194–2215, 2017.

[10] W. Duncan, J. Best, M. Golubitsky, H. F. Nijhout, and M. Reed. Homeostasis despite instability. *Mathematical Biosciences*, 300:130–137, 2018.

[11] William Duncan and Martin Golubitsky. Coincidence of homeostasis and bifurcation in feedforward networks. *International Journal of Bifurcation and Chaos*, 29(13):1930037, 2019.

[12] F. L. Eldridge, D. Paydarfar, P. G. Wagner, and R. T. Dowell. Phase resetting of respiratory rhythm: effect of changing respiratory "drive". *American Journal of Physiology-Regulatory, Integrative and Comparative Physiology*, 257(2):R271–R277, 1989.

[13] G Bard Ermentrout and David H Terman. *Mathematical foundations of neuroscience*, volume 35. Springer Science & Business Media, 2010.

[14] K. A. E. Geitz, D. W. Richter, and A. Gottschalk. The influence of chemical and mechanical feedback on ventilatory pattern in a model of the central respiratory pattern generator. In *Modeling and Control of Ventilation*, pages 23–28. Springer, 1995.

[15] Martin Golubitsky and Ian Stewart. Homeostasis, singularities, and networks. *Journal of mathematical biology*, 74(1-2):387–407, 2017.

[16] Martin Golubitsky and Ian Stewart. Homeostasis with multiple inputs. *Siam Journal on Applied Dynamical Systems*, 17(2):1816–1832, 2018.

[17] Martin Golubitsky and Yangyang Wang. Infinitesimal homeostasis in three-node input–output networks. *Journal of Mathematical Biology*, 80(4):1163–1185, 2020.

[18] Fred S Grodins, John S Gray, Karl R Schroeder, Arthur L Norins, and Richard W Jones. Respiratory responses to co2 inhalation. a theoretical study of a nonlinear biological regulator. *Journal of applied physiology*, 7(3):283–308, 1954.

[19] Auke Jan Ijspeert. A connectionist central pattern generator for the aquatic and terrestrial gaits of a simulated salamander. *Biological cybernetics*, 84(5):331–348, 2001.

[20] Eugene M Izhikevich. *Dynamical systems in neuroscience*. MIT press, 2007.

[21] D.W. Jordan and P. Smith. *Nonlinear Ordinary Differential Equations*. Oxford University Press, 4 edition, 2007.

[22] Oliver Junge, Oliver Schütze, Gary Froyland, Sina Ober-Blöbaum, and Kathrin Padberg-Gehle. *Advances in Dynamics, Optimization and Computation: A volume dedicated to Michael Dellnitz on the occasion of his 60th birthday*, volume 304. Springer Nature, 2020.

[23] Rose Anne Kenny, John Bayliss, Ann Ingram, and Richard Sutton. Head-up tilt: a useful test for investigating unexplained syncope. *The Lancet*, 327(8494):1352–1355, 1986.

[24] Arthur D Kuo. The relative roles of feedforward and feedback in the control of rhythmic movements. *Motor control*, 6(2):129–145, 2002.

[25] Yoshiki Kuramoto. *Chemical oscillations, waves, and turbulence*. Springer-Verlag, 1984.

[26] David N Lyttle, Jeffrey P Gill, Kendrick M Shaw, Peter J Thomas, and Hillel J Chiel. Robustness, flexibility, and sensitivity in a multifunctional motor control model. *Biological cybernetics*, 111(1):25–47, 2017.

[27] Yaroslav I Molkov, Jonathan E Rubin, Ilya A Rybak, and Jeffrey C Smith. Computational models of the neural control of breathing. *Wiley Interdisciplinary Reviews: Systems Biology and Medicine*, 9(2):e1371, 2017.

[28] Yaroslav I Molkov, Natalia A Shevtsova, Choongseok Park, Alona Ben-Tal, Jeffrey C Smith, Jonathan E Rubin, and Ilya A Rybak. A closed-loop model of the respiratory system: focus on hypercapnia and active expiration. *PloS one*, 9(10):e109894, 2014.

[29] Peter R Morrison. Temperature regulation in three central american mammals. *Journal of cellular and comparative physiology*, 27(3):125–137, 1946.

[30] H Frederik Nijhout, Janet Best, and Michael C Reed. Escape from homeostasis. *Mathematical biosciences*, 257:104–110, 2014.

[31] H Frederik Nijhout, Janet A Best, and Michael C Reed. Systems biology of robustness and homeostatic mechanisms. *Wiley Interdisciplinary Reviews: Systems Biology and Medicine*, 11(3):e1440, 2019.

[32] Mette S Olufsen, Johnny T Ottesen, Hien T Tran, Laura M Ellwein, Lewis A Lipsitz, and Vera Novak. Blood pressure and blood flow variation during postural change from sitting to standing: model development and validation. *Journal of applied physiology*, 99(4):1523–1537, 2005.

[33] Youngmin Park, Kendrick M Shaw, Hillel J Chiel, and Peter J Thomas. The infinitesimal phase response curves of oscillators in piecewise smooth dynamical systems. *European Journal of Applied Mathematics*, 29(5):905–940, 2018.

[34] Michael Reed, Janet Best, Martin Golubitsky, Ian Stewart, and H Frederik Nijhout. Analysis of homeostatic mechanisms in biochemical networks. *Bulletin of Mathematical Biology*, 79(9):2534–2557, 2017.

[35] Jonathan E Rubin, Bartholomew J Bacak, Yaroslav I Molkov, Natalia A Shevtsova, Jeffrey C Smith, and Ilya A Rybak. Interacting oscillations in neural control of breathing: modeling and qualitative analysis. *Journal of computational neuroscience*, 30(3):607–632, 2011.

[36] M. Sammon. Geometry of respiratory phase switching. *Journal of Applied Physiology*, 77(5):2468–2480, 1994.

[37] M. Sammon. Symmetry, bifurcations, and chaos in a distributed respiratory control system. *Journal of Applied Physiology*, 77(5):2481–2495, 1994.

[38] Kendrick M Shaw, David N Lyttle, Jeffrey P Gill, Miranda J Cullins, Jeffrey M McManus, Hui Lu, Peter J Thomas, and Hillel J Chiel. The significance of dynamical architecture for adaptive responses to mechanical loads during rhythmic behavior. *Journal of computational neuroscience*, 38(1):25–51, 2015.

[39] Sho Shirasaka, Wataru Kurebayashi, and Hiroya Nakao. Phase reduction theory for hybrid nonlinear oscillators. *Physical Review E*, 95(1):012212, 2017.

[40] Abigail C Snyder and Jonathan E Rubin. Conditions for multi-functionality in a rhythm generating network inspired by turtle scratching. *The Journal of Mathematical Neuroscience (JMN)*, 5(1):1–34, 2015.

[41] Lucy E Spardy, Sergey N Markin, Natalia A Shevtsova, Boris I Prilutsky, Ilya A Rybak, and Jonathan E Rubin. A dynamical systems analysis of afferent control in a neuromechanical model of locomotion: Ii. phase asymmetry. *Journal of neural engineering*, 8(6):065004, 2011.

[42] Yangyang Wang, Jeffrey P Gill, Hillel J Chiel, and Peter J Thomas. Shape versus timing: linear responses of a limit cycle with hard boundaries under instantaneous and static perturbation. *SIAM Journal on Applied Dynamical Systems*, 20(2):701–744, 2021.

[43] Yangyang Wang, Zhengyuan Huang, Fernando Antoneli, and Martin Golubitsky. The structure of infinitesimal homeostasis in input–output networks. *Journal of Mathematical Biology*, 82(7):1–43, 2021.

[44] Stephen Wiggins. *Normally Hyperbolic Invariant Manifolds in Dynamical Systems*. Number 105 in Applied Mathematical Sciences. Springer-Verlag, 1994.

[45] Zhuojun Yu and Peter J Thomas. Dynamical consequences of sensory feedback in a half-center oscillator coupled to a simple motor system. *Biological Cybernetics*, 115(2):135–160, 2021.